# Simultaneous inversion of active and passive source datasets for 3-D seismic structure with application to Tasmania

N. Rawlinson[1] and M. Urvoy[2]

Received 14 September 2006; revised 12 November 2006; accepted 22 November 2006; published 23 December 2006.

[1] Refraction, wide-angle reflection and teleseismic arrival time data are combined in a simultaneous inversion for 3-D lithospheric *P*-wavespeed and Moho geometry beneath Tasmania, southeast Australia. A new iterative nonlinear tomography scheme, which incorporates a novel grid-based method of traveltime prediction, is used to obtain the solution model. Synthetic resolution tests demonstrate that the crucial issue of trade-off between interface depth and layer velocity is satisfactorily resolved. In contrast to previous results from separate inversions of the active and passive source datasets, the new images reveal a zone of elevated wavespeed beneath the Cambrian Mt. Read Volcanics, and indicate that both crustal thinning and elevated wavespeeds occur beneath northeast Tasmania, which supports the case for the existence of a prior passive margin. Otherwise, most major inferences from the previous studies, including evidence for remnant subduction and crustal shortening, are supported by the new results. **Citation:** Rawlinson, N., and M. Urvoy (2006), Simultaneous inversion of active and passive source datasets for 3-D seismic structure with application to Tasmania, *Geophys. Res. Lett.*, *33*, L24313, doi:10.1029/2006GL028105.

## 1. Introduction

[2] Seismic body wave tomography is a well established tool for imaging subsurface seismic structure at a variety of scales, but most applications involve a single type of dataset, such as local earthquake [*Zhao et al.*, 1992; *Graeber and Asch*, 1999], teleseismic [*Steck et al.*, 1998; *Rawlinson et al.*, 2006] or refraction and wide-angle reflection [*Zelt et al.*, 1999; *Rawlinson et al.*, 2001]. When multiple datasets that span a common region are available, a combined inversion would in many cases be preferable to separate inversions, as the improved path coverage may result in a better constrained model. To date, a number of studies have attempted joint inversion of multiple datasets. For example, *Thurber* [1983] and *Ankeny et al.* [1986] include refraction traveltimes from several explosive sources in local earthquake tomography studies; *Parsons and Zoback* [1997] and *Eberhart-Phillips and Bannister* [2002] combine airgun and local earthquake traveltimes to constrain crustal structure; *Sato et al.* [1996] and *Zhao et al.* [1997] simultaneously invert local earthquake and teleseismic traveltimes for crust and upper mantle structure; and *West et al.* [2004] use both surface and body wave data in a joint inversion for crust and mantle structure.

[3] In this study, we simultaneously invert refraction (*Pg* and *Pn*), wide-angle reflection (*PmP*) and teleseismic data recorded by two separate experiments in order to image 3-D variations in lithospheric *P*-wavespeed and Moho structure beneath Tasmania. The crossing path coverage of the teleseismic dataset is extensive in the lower crust and upper mantle (between about 15–200 km depth) but virtually nonexistent in the mid-upper crust. In contrast, the path coverage of the active source dataset is almost exclusively crustal, with some penetration of the uppermost mantle. *Pg* traveltimes are sensitive to mid-upper crustal velocity structure, *PmP* traveltimes are most sensitive to variations in Moho geometry, while *Pn* traveltimes are sensitive to Moho geometry, crustal velocity and uppermost mantle velocity.

[4] Previously, the *PmP* and *Pn* traveltimes have been inverted for Moho structure [*Rawlinson et al.*, 2001], and the teleseismic arrival time residuals have been inverted for 3-D variations in wavespeed [*Rawlinson et al.*, 2006]. In the former case, it was found that there was insufficient path coverage to justify inverting for lateral velocity variation in addition to Moho structure, and in the latter case, the teleseismic dataset cannot resolve shallow crustal structure or the trade-off between Moho geometry and velocity. The potential for mapping crustal anomalies into the upper mantle with teleseismic tomography is well known, even with the use of station correction terms. *Waldhauser et al.* [2002] show that the inclusion of an accurate a priori crustal model is a highly effective way of mitigating this problem. Thus, a simultaneous inversion of the active and passive source datasets promises to yield a much improved result, as the teleseisms combined with the crustal refraction and reflections should be sufficient to constrain crustal velocity and Moho structure, which in turn means that teleseismic arrival time residual contributions from the crust will have less influence on the recovery of structure in the mantle.

[5] The island of Tasmania lies at the southern tip of the Tasman Orogen [*Betts et al.*, 2002], which comprises the eastern third of the Australian continent, and formed largely as a result of subduction related accretion in the Palaeozoic. The geological relationship between Tasmania and mainland Australia appears enigmatic [e.g., *Elliot et al.*, 1991], in particular due to the presence of Proterozoic outcrop in western Tasmania which predates the exclusively Phanerozoic rocks found on the adjacent mainland. Although there is no general agreement as to the tectonic assemblage of western Tasmania [*Rawlinson et al.*, 2006], there is little doubt that it largely occurred during the Middle to Late Cambrian Tyennan Orogeny. Eastern Tasmania contains no evidence of the Tyennan Orogeny or Proterozoic outcrop, and there has been much debate about the nature of the

[1] Research School of Earth Sciences, Australian National University, Canberra, ACT, Australia.
[2] Laboratoire de Geologie, Ecole Normale Superieure, Paris, France.


0094-8276/06/2006GL028105$05.00

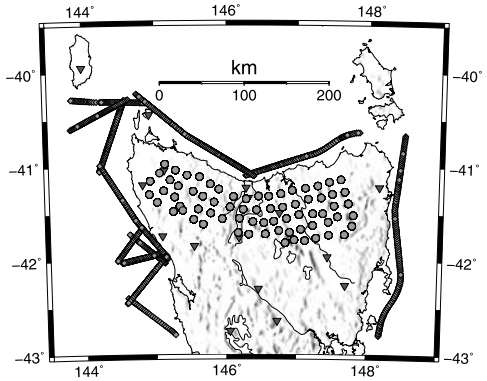


**Figure 1.** Map showing locations of passive seismic stations (grey circles), shot lines (contiguous grey diamonds) and active source receivers (dark grey triangles) used in this study.

transition between the two terranes [*Elliot et al.*, 1991; *Leaman*, 1994]. Seismic tomography is therefore well placed to contribute towards an improved understanding of Tasmanian geology and tectonic history.

## 2. Data and Method

[6] During the 1995 TASGO project, 44 analogue and digital seismometers were distributed throughout Tasmania to record approximately 36,000 airgun shots fired offshore in a complete circumnavigation of Tasmania (Figure 1). In their inversion for Moho structure, *Rawlinson et al.* [2001] used a total of 2148 *PmP* and 442 *Pn* traveltimes recorded at 21 receivers from 13 shot lines. Due to the location of the teleseismic array, which does not extend into southern Tasmania, we restrict our study to the northern half of Tasmania. Therefore, 1620 *PmP* and 402 *Pn* traveltimes recorded at 16 receivers from 12 shot lines are used (see Figure 1). However, since lateral velocity variations within the crust are now included, 1150 *Pg* traveltimes have been added.

[7] *Rawlinson et al.* [2006] use 6520 arrival time residuals from 101 teleseismic events in an inversion for the 3-D *P*-wavespeed structure beneath northern Tasmania. The dataset was recorded by an array of 72 vertical component short period and three component broadband seismometers that was deployed in northern Tasmania (Figure 1) for a period of approximately five months during 2002. A majority of the phases used were direct *P*, but the dataset also includes several *pP*, *PP*, *PcP*, *ScP* and *PKiKP* phases. Most of the teleseismic events are distributed to the north and east of the array, with relatively few lying to the south and west [see *Rawlinson et al.*, 2006, Figure 4]. We combine this dataset with the active source dataset, resulting in a total of 9692 *P*-wave traveltimes and arrival time residuals available for use in the simultaneous inversion.

[8] We apply a new tomographic inversion scheme that has been designed for the integration of multiple classes of body wave datasets. The central innovation of the scheme is its use of a grid based eikonal solver, known as the fast marching method or FMM [*Sethian and Popovici*, 1999; *Rawlinson and Sambridge*, 2004], to solve the forward problem of traveltime prediction. In a recent paper, *de Kool et al.* [2006] develop a multi-stage FMM in 3-D spherical coordinates, which allows phases comprising any number of refraction and reflection branches to be tracked in heterogeneous layered media with undulating interfaces. A variety of arrivals, including reflection multiples, converted waves, local earthquake phases and teleseisms can be computed through complex structures such as subduction zones. The computational efficiency and robustness of the multi-stage FMM make it well suited to large tomographic problems.

[9] The iterative non-linear inversion scheme allows velocity, interface depth and source location parameters to be inverted for. Each layer is independently defined by a 3-D regular grid of velocity nodes, with cubic B-splines used to describe a smoothly varying velocity field. Likewise, each layer boundary is independently defined by a 2-D grid of interface depth nodes, with cubic B-splines used to generate a smoothly varying surface. A subspace inversion scheme similar to the one used by *Rawlinson et al.* [2006] is applied to solve the inverse problem of adjusting model parameters to better satisfy data observations subject to regularization constraints. In this case, both damping and smoothing are used to help minimize solution non-uniqueness. A series of inversions were performed with different levels of damping and smoothing in order to identify the model with minimum perturbation and roughness that still satisfies the data to an acceptable level. The multi-stage FMM scheme and subspace method are applied iteratively in order to address the non-linear nature of the inverse problem.

## 3. Results and Discussion

[10] We represent the seismic structure of the Tasmanian lithosphere with a two layer crust and upper mantle model in spherical coordinates. Both layers are independently defined using velocity grids with a node separation of approximately 10 km in all three dimensions. The interface grid, which describes the spatial variations of the Moho, is defined using the same node separation in latitude and longitude as the velocity grid. The initial or starting model has velocity in the upper mantle defined by the global reference model *ak*135, and velocity varying with depth in the crust according to a locally derived 1-D model [*Rawlinson et al.*, 2001, 2006] which also estimates Moho depth to be 29 km. The velocity contrast across the Moho is approximately 1.5 km/s.

### 3.1. Synthetic Tests

[11] Before presenting results from the combined datasets, we first investigate solution non-uniqueness, which arises from the under-determined nature of the inverse problem. This is done using synthetic checkerboard tests (Figure 2), which are based on input models defined by alternating regions of high and low velocity (between ±400 m/s) and deep and shallow Moho (between 23–35 km depth). The aim is to try and recover this pattern from a dataset obtained by solving the forward problem with identical sources, receivers and phase types to that of the observed data. In order to simulate the noise content of the observations, Gaussian noise with a standard deviation of 77 ms and 100 ms is added to the teleseismic arrival time residuals and active source traveltimes respectively.

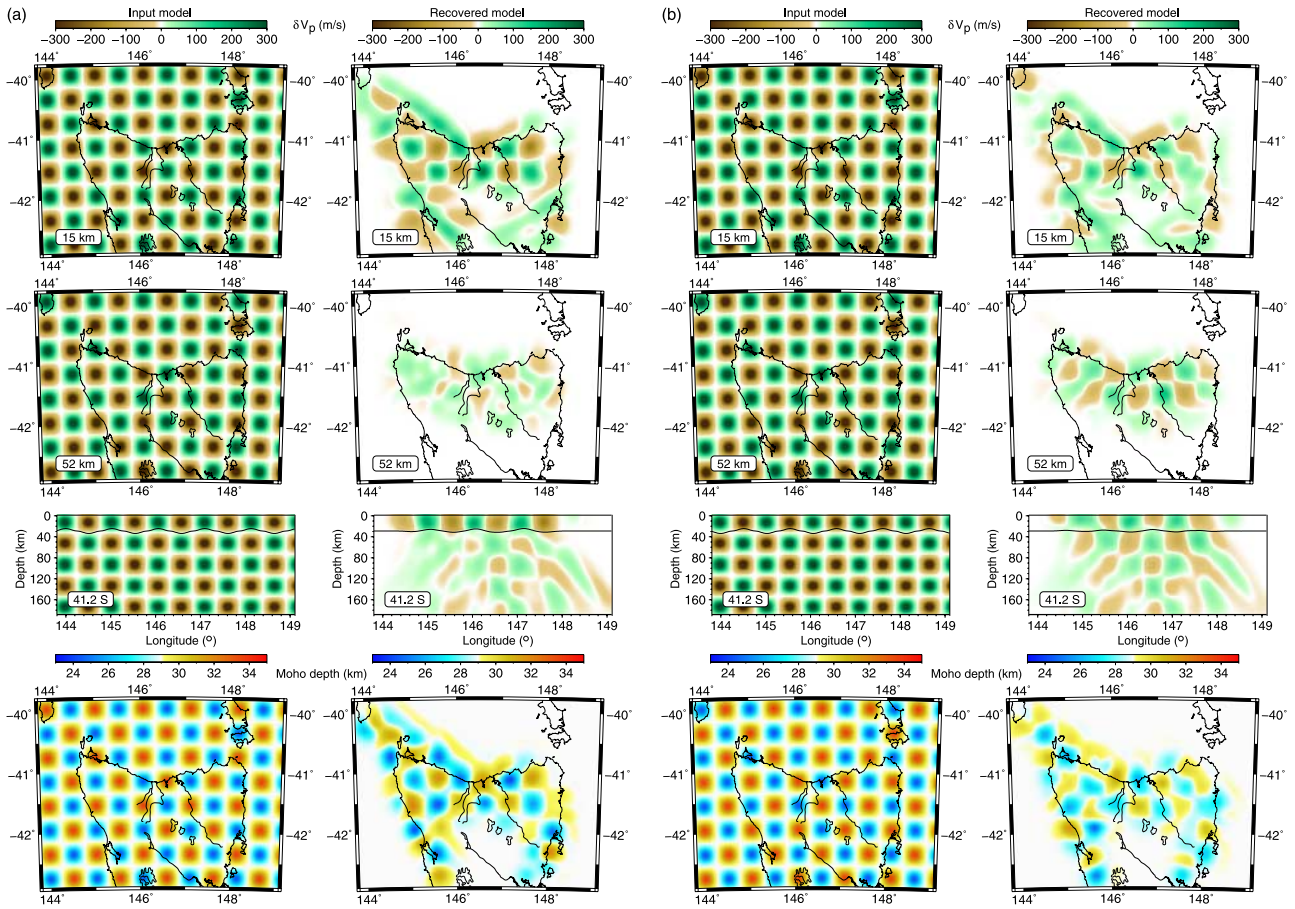


**Figure 2.** Results of two synthetic checkerboard tests used to examine solution robustness. (a) Input and recovered models for first test; (b) input and recovered models for second test, which differs from the first by using an inverted pattern of Moho perturbations. In both Figures 2a and 2b, the first two rows show horizontal slices, the third row shows a vertical east-west slice, and the fourth row illustrates Moho depth.

[12] The first checkerboard test (Figure 2a) aligns the shallow and deep Moho perturbations with the positive and negative wavespeed anomalies in the crust respectively, as illustrated by the E–W depth slice in Figure 2a. Correspondingly, the shallow and deep Moho perturbations align with negative and positive wavespeed anomalies in the uppermost mantle respectively. Six iterations of the tomographic inversion scheme are applied to obtain a solution model, which satisfies the synthetic dataset to the level of the imposed Gaussian noise. The quality of the recovered checkerboard pattern (Figure 2a, right) within the crust and along the Moho in the vicinity of the teleseismic array is generally good. In regions spanned only by the refraction and wide-angle reflection dataset, however, the recovery is not as successful. This highlights the importance of the teleseismic dataset in the accurate recovery of crustal structure. Within the upper mantle beneath the teleseismic array, the recovery of the checkerboard is less successful, although the basic pattern is still evident.

[13] A second checkerboard test (Figure 2b) is performed which differs from the first test only in that the Moho checkerboard pattern is overturned. Thus, the negative and positive wavespeed anomalies in the crust now overlie the shallow and deep Moho perturbations respectively, and a similar pattern reversal occurs between the Moho and uppermost mantle. As in the first example, six iterations of the inversion scheme are required to satisfy the synthetic dataset to the level of the imposed noise. The recovered model (Figure 2b, right) differs in character from the previous test solution (Figure 2a, right). In particular, the pattern of anomalies in the uppermost mantle is recovered more accurately (cf. 52 km depth slice of Figure 2b with Figure 2a). Conversely, the crustal velocity anomalies are more poorly recovered, and the Moho perturbations have a lower amplitude.

[14] The differences between the results of the two synthetic tests can be largely attributed to the imperfect resolution of the interface depth and layer velocity trade-off. In the first test (Figure 2a), the teleseismic arrival time residuals have significant positive or negative contributions from the crust. The second test (Figure 2b) inverts the Moho checkerboard pattern so that the teleseismic arrival time residual component from the interface perturbation is partially neutralized by the overlying crustal velocity anomaly. Consequently, there is a smaller shallow contribution to the arrival time residual that can get smeared back into the upper mantle, which is why this region of the model is better resolved in Figure 2b than Figure 2a. Also, the lack of

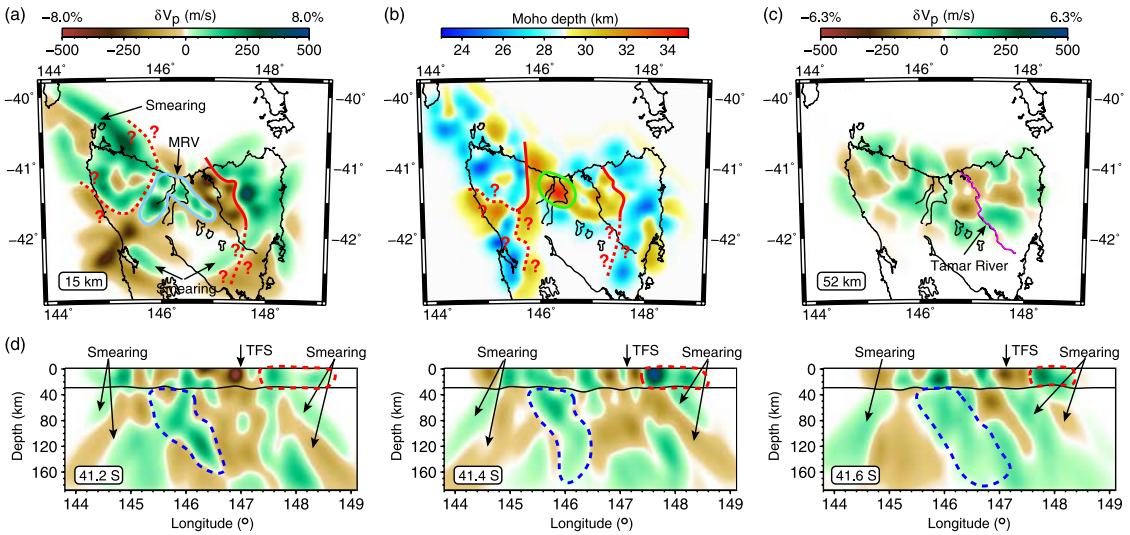


**Figure 3.** Summary of Tasmania tomography results. (a) Crustal section at 15 km depth; (b) Moho structure; (c) upper mantle section at 52 km depth; (d) three east-west cross-sections. Several features commented on in the main text are highlighted. Note that the scale bar for the velocity slices is identical to that used in the synthetic tests, except that it has been extended to ±500 m/s to account for several strong perturbations in the crust. TFS = Tamar Fracture System; MRV = Mt. Read Volcanics.

a substantial shallow component to the teleseismic residual means that they do not require the starting model for the crust to be significantly perturbed in order to be satisfied. This would also explain why the crustal anomalies are not as well recovered in Figure 2b compared to Figure 2a.

[15] In summary, these tests show that seismic structure is adequately resolved by the combined datasets, particularly beneath regions of common array coverage. However, as with most tomography studies, the application of damping and smoothing to regularize the inversion has generally resulted in the recovered models underestimating the true amplitudes of the velocity and interface perturbations. This means that estimates of velocity and interface perturbation magnitudes beneath Tasmania are likely to be conservative. The rapidly undulating pattern of the velocity and interface checkerboard helps to emphasize the trade-off between interface depth and velocity variation; synthetic tests carried out with a variety of other structures show that this effect is usually less pronounced. Figures 2a and 2b can therefore be thought of as end-member models, with recovery of crust and upper mantle structure in most cases lying between what is indicated by these two solutions.

### 3.2. Lithospheric Structure of Tasmania

[16] The observed wide-angle and teleseismic datasets are inverted using the same inversion parameters (damping, smoothing, number of iterations etc.) as the synthetic datasets. The final solution model reduces the data misfit variance by 76% from 0.084 $s^2$ to 0.020 $s^2$, which corresponds to an RMS reduction from 290 ms to 140 ms. A series of slices through the solution model, with several notable features highlighted, are shown in Figure 3. One of the more prominent crustal anomalies is a strong W–E negative to positive velocity contrast (up to 1 km/s over several 10s of km) in northeast Tasmania (Figures 3a and 3d). This feature may extend further southward, as implied in Figure 3a, but a lack of resolution (see Figure 2) has resulted in significant smearing in this area. Figure 3b reveals that the region of elevated crustal velocity in the east is underlain by a shallow Moho, which does extend southward. However, limited path coverage makes it difficult to ascertain its true extent.

[17] *Rawlinson et al.* [2006] identified a similar region of elevated velocity east of the Tamar River from an inversion of the teleseismic dataset for velocity variation only. From an inversion of *Pn* and *PmP* traveltimes for Moho geometry only, *Rawlinson et al.* [2001] found inconclusive evidence for crustal thinning in the same region. Conceivably, a thinner crust could also have satisfied the teleseismic dataset, and higher crustal velocities could also have satisfied the *Pn* and *PmP* traveltimes. Our new model from the simultaneous inversion shows that both a thinning of the crust and elevated crustal velocities are required to satisfy the combined datasets. This helps to confirm the hypothesis that eastern Tasmania is underlain by rocks with an oceanic crustal affinity, which contrasts with the continentally derived siliciclastic core of western Tasmania [*Rawlinson et al.*, 2006]. It has been suggested that this region of Tasmania began as a passive margin [*Reed*, 2001] in the Ordovician, with subsequent episodes of orogenesis and sedimentation compressing and thickening the oceanic crust. Interestingly, the so-called Tamar Fracture System or TFS (approximately coincident with the Tamar River in Figure 3), which has traditionally been used to mark the boundary between the Eastern and Western Tasmania Terranes, does not overly the velocity or interface depth variation (Figure 3d). This corroborates the view of *Leaman* [1994] that the TFS is a shallow feature unrelated to the terrane boundary at depth.

[18] Further west, there is a prominent and well resolved region of thicker crust beneath central northern Tasmania (Figure 3b). A similar feature is observed in the Moho model of *Rawlinson et al.* [2001], and is probably related to crustal shortening associated with the Tabberabberan Orog-

eny, which affected much of eastern Australia during the Mid Devonian.

[19] The pattern of anomalies in the upper mantle (Figure 3c) is quite different from that of the crust; in particular, the strong velocity contrast identified beneath northeast Tasmania is no longer present. One prominent upper mantle structure is an easterly dipping zone of higher velocity (Figure 3d), which becomes more diffuse further south. This feature is located in a well constrained region of the model, and is unlikely to be an artifact related to smearing. Although slightly different in shape, *Rawlinson et al.* [2006] also image this anomaly, and suggest that it may represent remnants of a Mid Cambrian easterly dipping subduction zone. This is significant, because the adjacent mainland Delamerian Orogen is thought to have involved easterly dipping subduction, and recently boninites of a similar age and composition have been found in both locations [*Direen and Crawford*, 2003]. Historically, the tectonic relationship between Tasmania and mainland Australia has always been uncertain, but these results help to reinforce the view that they have been linked since at least the early Palaeozoic.

[20] Beneath northwest Tasmania, there is a broad region of shallow Moho which is overlain by a zone of higher velocity crust (see Figures 3a and 3b). Although similar to the earlier results [*Rawlinson et al.*, 2001, 2006], the shallow Moho now extends further south and east. There may well be an association between this change in crustal seismic character and the easterly dipping structure identified in the mantle beneath. Cambrian ophiolites are exposed on the surface along the eastern margin of the thinner, higher velocity crust, which helps support the argument for a prior collision zone in this region.

[21] As outlined above, our new imaging results retain most of the basic features that are present in the separately derived Moho and velocity models of *Rawlinson et al.* [2001] and *Rawlinson et al.* [2006]. It is chiefly the differences in the finer scale anomalies that set the models apart, particularly within the crust. For example, the high velocity anomaly marked MRV in Figure 3a spatially correlates with the surface exposure of the Cambrian Mt. Read Volcanics, a highly mineralized metal province; this is not observed in either of the two earlier models. Also, the amplitudes of the crustal anomalies are generally greater than those found in the velocity model of *Rawlinson et al.* [2006].

## 4. Conclusions

[22] We have used a new iterative non-linear tomography scheme to simultaneously invert active (refraction, wide-angle reflection) and passive (teleseismic) source datasets for the 3-D seismic structure of the Tasmanian lithosphere. Careful analysis of synthetic checkerboard test results reveal that although trade-off between velocity and interface depth is present, it is resolved to an acceptable level. First-order features of the solution model are in broad agreement with those of previous studies, which separately inverted *Pn* and *PmP* traveltimes and teleseismic arrival time residuals for Moho structure and lithospheric velocity respectively. At smaller scales, the combined inversion results reveal several new structures, including a high velocity anomaly beneath the Mt. Read Volcanics.

## References


Ankeny, L. A., L. W. Braile, and K. H. Olsen (1986), Upper crustal structure beneath the Jemez Mountains volcanic field, New Mexico, determined by three-dimensional simultaneous inversion of seismic refraction and earthquake data, *J. Geophys. Res.*, *91*, 6188–6198.

Betts, P. G., D. Giles, G. S. Lister, and L. Frick (2002), Evolution of the Australian lithosphere, *Aust. J. Earth Sci.*, *49*, 661–695.

de Kool, M., N. Rawlinson, and M. Sambridge (2006), A practical grid based method for tracking multiple refraction and reflection phases in three-dimensional heterogeneous media, *Geophys. J. Int.*, *167*, 253–270.

Direen, N. G., and A. J. Crawford (2003), The Tasman Line: Where is it, what is it, and is it Australia's Rodinian breakup boundary?, *Aust. J. Earth Sci.*, *50*, 491–502.

Eberhart-Phillips, D., and S. Bannister (2002), Three-dimensional crustal structure in the Southern Alps region of New Zealand from inversion of local earthquake and active source data, *J. Geophys. Res.*, *107*(B10), 2262, doi:10.1029/2001JB000567.

Elliot, C. G., D. R. Gray, and N. B. Woodward (1991), Relating Tasmania to the Lachlan Fold Belt, in *Tectonics and Mineralization of the Lachlan Fold Belt*, vol. 29, p. 15, Geol. Soc. of Aust., Sydney, N. S. W., Australia.

Graeber, F. M., and G. Asch (1999), Three-dimensional models of *P* wave velocity and *P*-to-*S* velocity ratio in the southern central Andes by simultaneous inversion of local earthquake data, *J. Geophys. Res.*, *104*, 20,237–20,256.

Leaman, D. E. (1994), The Tamar Fracture System in Tasmania: Does it exist?, *Aust. J. Earth Sci.*, *41*, 73–74.

Parsons, T., and M. L. Zoback (1997), Three-dimensional upper crustal velocity structure beneath San Francisco Peninsula, California, *J. Geophys. Res.*, *102*, 5473–5490.

Rawlinson, N., and M. Sambridge (2004), Multiple reflection and transmission phases in complex layered media using a multistage fast marching method, *Geophysics*, *69*, 1338–1350.

Rawlinson, N., G. A. Houseman, C. D. N. Collins, and B. J. Drummond (2001), New evidence of Tasmania's tectonic history from a novel seismic experiment, *Geophys. Res. Lett.*, *28*, 3337–3340.

Rawlinson, N., A. M. Reading, and B. L. N. Kennett (2006), Lithospheric structure of Tasmania from a novel form of teleseismic tomography, *J. Geophys. Res.*, *111*, B02301, doi:10.1029/2005JB003803.

Reed, A. R. (2001), Pre-Tabberabberan deformation in eastern Tasmania: A southern extension of the Benambran Orogeny, *Aust. J. Earth Sci.*, *48*, 785–796.

Sato, T., M. Kosuga, and K. Tanaka (1996), Tomographic inversion for *P* wave velocity structure beneath the northeastern Japan arc using local and teleseismic data, *J. Geophys. Res.*, *101*, 17,597–17,615.

Sethian, J. A., and A. M. Popovici (1999), 3-D traveltime computation using the fast marching method, *Geophysics*, *64*, 516–523.

Steck, L. K., C. H. Thurber, M. Fehler, W. J. Lutter, P. M. Roberts, W. S. Baldridge, D. G. Stafford, and R. Sessions (1998), Crust and upper mantle *P* wave velocity structure beneath Valles caldera, New Mexico: Results from the Jemez teleseismic tomography experiment, *J. Geophys. Res.*, *103*, 24,301–24,320.

Thurber, C. H. (1983), Earthquake locations and three-dimensional crustal structure in the Coyote Lake area, central California, *J. Geophys. Res.*, *88*, 8226–8236.

Waldhauser, F., R. Lippitsch, E. Kissling, and J. Ansorge (2002), High-resolution teleseismic tomography of upper-mantle structure using an a priori three-dimensional crustal model, *Geophys. J. Int.*, *150*, 403–414.

West, M., W. Gao, and S. Grand (2004), A simple approach to the joint inversion of seismic body and surface waves applied to the southwest U.S., *Geophys. Res. Lett.*, *31*, L15615, doi:10.1029/2004GL020373.

Zelt, C. A., A. M. Hojka, E. R. Flueh, and K. D. McIntosh (1999), 3D simultaneous seismic refraction and reflection tomography of wide-angle data from the central Chilean margin, *Geophys. Res. Lett.*, *26*, 2577–2580.

Zhao, D., A. Hasegawa, and S. Horiuchi (1992), Tomographic imaging of *P* and *S* wave velocity structure beneath northeastern Japan, *J. Geophys. Res.*, *97*, 19,909–19,928.

Zhao, D., Y. Xu, D. Wiens, L. Dorman, J. Hildebrand, and S. Webb (1997), Depth extent of the Lau back-arc spreading center and its relation to subduction processes, *Science*, *278*, 254–257.



N. Rawlinson, Research School of Earth Sciences, Australian National University, Canberra, ACT 0200, Australia. (nick@rses.anu.edu.au)

M. Urvoy, Laboratoire de Geologie, Ecole Normale Superieure, F-75005 Paris, France.